Catalysis Science & Technology

Accepted Manuscript

ROYAL SOCIETY OF CHEMISTRY

www.rsc.org/catalysis

COMBINED STEAM AND CARBON DIOXIDE REFORMING OF METHANE OVER POROUS NICKEL BASED CATALYSTS

M.M. Danilova[1], Z.A. Fedorova[1,*], V.A. Kuzmin[1], V.I. Zaikovskii[1], A.V. Porsin[1], T.A. Krieger[1,2]

Abstract

The phase composition and texture of nickel catalysts supported on porous nickel ribbon with a MgO underlayer were studied. In the supported reduced catalysts (900ºC, H_2), nickel crystallites were epitaxially bound with MgO. The reaction of combined steam and carbon dioxide reforming of methane to synthesis gas (750ºC, $CH_4/CO_2/H_2O/N_2$ = 35/23/39/3, GHSV = 62.5 L/g h) was performed in flow reactor in the presence of the developed catalysts. The catalysts with the MgO underlayer completely covering the nickel ribbon showed stable activity throughout the test period (18h); after the reaction no carbon deposits were found in them. The resistance of these catalysts to carbonization was attributed both to the formation of nickel crystallites epitaxially bound with MgO and to the formation of the MgO underlayer that covers the nickel ribbon and prevents its contact with the reaction medium. Based on the supported nickel catalyst the monolithic catalyst was prepared and tested in the developed flow reactor. According to the test data, methane conversion on the monolithic catalyst at a contact time 0.29 s was not lower than 94 % and the synthesis gas yield was 90%; at this contact time experimental values are close to the calculated equilibrium values.

1. Introduction

The combined steam and carbon dioxide reforming (SCDR) of methane to synthesis gas attracts much attention in the recent years. This process allows to convert two major greenhouse gases in synthesis gas. In comparison with dry reforming of methane, the addition of steam in the feed for CO_2-reforming reduces the formation of carbon.[1-3] By changing the H_2O/CO_2 ratio in the reaction feed, the H_2/CO product ratio can be controlled,[1-3] and this makes it possible to produce synthesis gas with the H_2/CO ratio of about 2, which is suitable for the oxo- and Fisher-Tropsch synthesis processes.[4,5] The SCDR of methane enables the production of synthesis gas from such renewable energy sources as biogas, whose main components are methane, carbon dioxide and water.

[1]*Boreskov Institute of Catalysis SB RAS*

[2]*Novosibirsk State University*

[*]Corresponding author. Fax: +738333269402

E-mail address: sabirova@catalysis.ru (Fedorova Z.A.)

According to the literature available the main direction of development of catalysts for SCDR of methane is associated with supported nickel catalysts. Nickel catalysts are active and selective in this process and are less expensive than catalysts containing platinum group metals. The characteristic drawback of nickel catalysts is their carbonization, which leads to a decrease in their activity.[1,3,6-12]

The carbonization of nickel catalysts can be diminished by the addition of promoters, such as calcium oxide,[1,7,8,10] magnesium oxide,[3,6,8,11] oxides of rare earth elements,[8] noble metals[12] and by optimization of synthesis methods.[13,14]

The implementation of the endothermic reactions of SCDR of methane requires an intensive heat transfer from an external source into the reaction zone and the equalization of the temperature inside the catalyst bed. It means that the catalysts for these reactions must have high thermal conductivity, which can be imparted by the use of metallic supports.[15,16] A number of catalysts on such supports were tested in the steam reforming of methane: nickel composite catalyst reinforced with a stainless steel gauze,[17,18] a nickel catalyst supported onto an oxide underlayer deposited on porous nickel,[19] a composite nickel catalyst obtained by the capsulation of lanthanum nickelate particles in metal-ceramics,[20] a nickel catalyst supported on a porous nickel plate with an underlayer of MgO.[21]

Analysis of published data shows that the use of MgO as an underlayer for the nickel catalysts is very promising: it has high thermal stability, reduces carbonization because of basic properties, and it easily forms solid solutions with NiO owing to the similarity of the structural parameters, which facilitates the formation of dispersed crystallites of reduced nickel.[5,22] A number of supported nickel catalysts with a MgO underlayer have been studied: nickel catalysts supported on metal foams,[23] porous nickel plate,[21] α-Al_2O_3,[6] and Al_2O_3-SiO_2.[8,9]

The aim of the current investigation was to elucidate the catalytic properties of nickel catalysts supported on porous nickel ribbon with a MgO underlayer including monolithic catalyst in the SCDR of methane to synthesis gas.

2. Experimental

2.1. Catalyst preparation

The supported nickel catalysts were prepared on a 0.1 mm thick porous nickel ribbon (pNirb) obtained by rolling of a nickel powder followed by calcination at 1200°C in a H_2 flow.[24] The ribbon nickel support had a specific surface area of 0.15 m^2/g and the total pore volume of ca. 0.1 cm^3/g. The MgO underlayer was prepared by impregnating the nickel ribbon support with a $Mg(NO_3)_2$ solution followed by drying and then by calcination at 550°C in flowing H_2; the support I contained 6.0 wt.% MgO, the support II – 10.3 wt.% MgO. The decomposition of $Mg(NO_3)_2$ in air is a usual method for the preparation of MgO support,[6,9,23,25] but in the case of a nickel support, it can lead to loosening of the nickel surface.[26,27] Therefore, to reduce the loosening of the nickel ribbon surface, decomposition of

$Mg(NO_3)$ was carried out in a H_2 flow. Catalysts I and II were prepared by supporting of nickel on supports I and II via their impregnation with a mixture of $Ni(NO_3)_2$ and $Mg(NO_3)_2$ solutions. After impregnation, all the catalysts were dried and then calcined at 450°C in a N_2 flow. The prepared catalysts were reduced in flowing H_2 at 900°C for 1 h. The content of supported nickel in the reduced catalysts was 1-4 wt. %; the content of MgO in catalysts was 7-12 wt.%.

2.2. Characterization

The specific surface area and the pore radius distribution were determined by low-temperature nitrogen adsorption at 77 K using an ASAP–2400 (Micromeritics, USA) precision instrument. The error of the evaluation of the specific surface area did not exceed 5 rel.%. For some samples, the total pore volume and the pore radius distribution were determined using mercury porosimetry. Particle morphology was examined by scanning electron microscopy (SEM) and by transition electron microscopy (TEM) with the respective use of JSM-6460LV and JEM-2010 (JEOL Co., Japan) instruments with a lattice resolution of 0.14 nm. The energy dispersive X-ray microanalysis (EDX) of some samples was performed using an EDAX energy dispersive spectrometer with a Si(Li) detector with an energy resolution of 130 eV. Crystal faces were indexed by high resolution TEM (HRTEM) of lattice fringe images. Phase analysis was carried out using X-ray diffraction patterns taken with an ARLX´TRACT (Thermo, Switzerland) instrument (monochromatized CuK_α radiation).

2.3. Catalytic activity

Catalyst activity in the SCDR of methane was evaluated by the flow method under atmospheric pressure at 750°C using a conventional continuous flow quartz reactor with an inner diameter of 14 mm. The initial reaction mixture comprised of 35 vol.% of CH_4, 23 vol.% of CO_2, 39 vol.% of H_2O, and 3 vol.% of N_2. According to,[1-3] such feed composition allows a production of synthesis gas with the H_2/CO ratio of about 2. The feed rate of the initial mixture was 25.0 L/h. For the catalytic activity measurements, ribbon catalysts were cut to pieces (1.5mm×1.5mm×0.1mm). Catalyst samples weighing 0.40 g were used in the tests. A commercial catalyst for steam reforming of methane NIAP-18 (10.5 wt.%Ni/Al_2O_3)[28] was used for the comparison. The catalyst sample weighing 0.40 g was tested in the form of a 0.25–0.50 mm fraction. Before the catalytic activity measurements, the samples were reduced in situ at 750°C in flowing H_2 for 1 h. Then hydrogen was substituted for the reaction mixture and measurements were taken after keeping the catalysts in the reaction mixture for 1 h. The catalyst bed temperature was controlled with a thermocouple mounted in the reactor at the level with the catalyst bed. The temperature evaluation error was ± 2°C. The composition of reaction mixtures was analyzed chromatographically: separation of oxygen, nitrogen and methane was performed using a column with NaX at room temperature, a heat conductivity detector, helium as a carrier gas; the concentrations of methane, carbon oxide, carbon

dioxide and hydrogen were measured on a chromatograph equipped with a heat conductivity detector and a temperature-programmed column (in a temperature range of 50-200°C) filled with activated carbon, argon served as a carrier gas; hydrocarbons were separated on a chromatograph equipped with a flame-ionization detector and a temperature-programmed column (in a temperature range of 50-200°C) filled with alumina, hydrogen as a carrier gas. The error of the chromatographic measurements was less than 10%.

Catalytic activity measurements in the empty reactor showed that the methane conversion in this case was less than 1%.

The supported nickel catalyst 4.0% Ni/(rpNi + 10.4% MgO) (I) was used to prepare a monolithic catalyst in the form of a rectangular block with the cross-section of 100 × 6 mm^2 and a height of 70 mm. The monolithic catalyst consisted of alternating corrugated (corrugation height of 1.8 mm, the base of the triangular channel of 4.0 mm) and smooth ribbons with the supported nickel catalyst.

The SCDR of methane to synthesis gas was performed in the developed flow reactor (Fig.1), which consisted of an evaporator 1 (cross-section of 20×90 mm^2, height of 70 mm), a reaction zone with the monolithic catalyst 2, and a gas burner 3 mounted successively in one housing. The monolithic catalyst was mounted in the center of the reaction zone. The fuel mixture (natural gas and air) was supplied to the burner (d = 100 mm) through a tube 4 (d = 20 mm) with several rows of holes (d = 2 mm). An additional flow of air was fed tangentially through the tube 5 (d = 8 mm), which facilitated the combustion. Ignition of the gas mixture was provided with an electro-spark between the tube 4 and electrode 6. Combustion products were directed to heat the reaction zone. The temperatures of the heating gases and the monolithic catalyst were measured using chromel-alumel thermocouples 7,8,9. The temperature of the heating gases measured before and after the reactor was 1070-1125°C and 860-930°C, respectively. The evaporator 1 contained plates (shelves) mounted at 10-mm intervals. Water entered the evaporator through a capillary 10 (d = 1 mm). The capillary was mounted inside a tube 11 (d = 5 mm) through which carbon dioxide was supplied. This design protected the capillary from the hot gases exiting the burner and prevented water from boiling, which could lead to a non-uniformity of the flow. After the evaporator, the mixture of water and carbon dioxide (12), with admixed methane 13, was fed into the reactor through a tube 14 (d = 5 mm). The tube contained holes (d = 1 mm) located at the opposite sides of the catalyst unit, which provided a better distribution of the reaction mixture over the reactor cross-section. The flows of gases and water were measured and adjusted with flow mass meters. The composition of reaction products was analyzed with a gas analyzer.

3. Results and Discussion

3.1. Phase composition and texture of initial catalysts

X-ray diffraction data showed that the metallic support contains only the nickel phase. Supports I and II contain phases of nickel and MgO with a = 4.219 Å (Table 1). One can assume that the obtained lattice parameter of MgO was higher than that given in[29] because of a lower degree of crystallinity and a higher degree of defects, which resulted from the formation of MgO in a hydrogen flow. In the reduced catalysts with supported nickel, the diffraction peaks correspond to only one oxide phase and nickel. Diffraction peaks of the oxide phases are very weak compared to the diffraction peaks of nickel and have an interjacent position between the peaks of pure oxides and are shifted to the diffraction peaks of MgO (Fig.2). According to,[31] this diffraction pattern indicates the formation of a solid solution of NiO in MgO. The formation of NiO in MgO solid solution at low calcination temperature, 500°C[32] and 400°C[33] was shown by X-ray diffraction in[32,33]. It is believed that the heating of supports I and II impregnated with a mixture of $Ni(NO_3)_2$ and $Mg(NO_3)_2$ solutions in N_2 flow at 450°C yields the dispersed solid solution of NiO in MgO. The presence of a phase of the solid solution after reduction treatment (900ºC, H_2) can be explained by hindered reduction of Ni^{2+} cations embedded into the lattice of hardly reducible MgO (the heat of formation of MgO is higher than that of NiO[34]). An increase in the temperature of NiO reduction after the formation of its solid solution in MgO is shown in.[9,22,35]

Table 1 Unit cell parameters of oxide phases in the samples.

Catalyst	a_{MgO} (Å)	$a_{Ni_XMg_{1-X}O}$ [1] (Å)	a_{NiO} (Å)
pNirb + 6.0% MgO (I)	4.219	-	-
pNirb + 10.3% MgO (II)	4.219	-	-
1.0% Ni/(pNirb + 6.7% MgO) (I)	-	4.210	-
2.7% Ni/(pNirb + 8.6% MgO) (I)	-	4.208	-
4.0% Ni/(pNirb + 10.4% MgO) (I)	-	4.208	-
2.3% Ni/(pNirb + 12.2% MgO) (II)	-	4.209	-
MgO	4.211[2]	-	-
NiO	-	-	4.177[3]

[1] $Ni_XMg_{1-X}O$ – assumed solid solution of NiO in MgO. [2] According to Ref.[29]

[3] According to Ref.[30]

The ribbon nickel support has a macroporous structure with a low total pore volume: according to the mercury porosimetry data, most pores have the radius from 5 to 60 μm. The macroporous nature of the support is confirmed by SEM data: the support has a corpuscular structure formed by rounded nickel particles with a size of 3-30 μm fused at the contact points.

According to SEM data, the MgO underlayer forms a loose porous layer with a thickness of 2-3 μm. According to the low-temperature nitrogen adsorption data, the specific surface area of support I is 7.5 m^2/g and of support II is 11 m^2/g (Table 2). The MgO underlayer in supports I and II has fine pores with an average diameter of 4-6 nm.

Table 2 Texture parameters of the catalysts.

Catalyst	S_{sq}, m^2/g	D_{Ni}, nm^2
pNirb + 6.0% MgO (I)[1]	7.5	-
pNirb + 10.3% MgO (II)[1]	11	-
1.0% Ni/(pNirb + 6.7% MgO) (I)	1.7	3-5
2.7% Ni/(pNirb+ 8.6% MgO) (I)	1.6	3-5
4.0% Ni/(pNirb + 10.4% MgO) (I)	1.9	3-7
1.2% Ni/(pNirb + 11.3% MgO) (II)	3.0	3-5
2.3% Ni/(pNirb + 12.2% MgO) (II)	-	3-5

[1]The samples were reduced at 750°C, H_2

[2]Dominant nickel particle size on the MgO surface according to TEM data.

As follows from the TEM images obtained, the MgO underlayer in supports I and II consists of aggregates 50-300 nm in size formed by primary 2-10-nm particles. The MgO underlayer does not contain separate nickel particles except for the sparse large (100 nm) particles probably detached from the nickel support during the sample preparation. Nevertheless, the EDX-spectra of MgO in supports I and II show Ni in the form of weak spectral lines corresponding to the Ni content not exceeding 2 at.% relative to Mg. The intensities of the nickel lines in the EDX spectra from different areas of the MgO surface are different, which indicates that during calcination, MgO non-uniformly interacts with the NiO film. Probably, the adjoined particles of MgO and NiO (Fig. 3) react to form a dispersed mixed oxide, whereas the particles of MgO that are not in contact with the surface of nickel ribbon do not contain dissolved nickel. The possibility of interaction of NiO with MgO during heating in hydrogen at temperatures of 250-400°C is shown in,[37] where the authors assumed that the diffusion of Ni^{2+} cations into the surface layer of MgO proceeds in parallel with their reduction. The same assumption can be made on the basis of the data in.[38] In addition, the calcination of the impregnated nickel ribbon leads to the decomposition of $Mg(NO_3)_2$ with the formation of nitrogen oxides, which are able to oxidize some parts of the nickel ribbon surface.

Impregnation of the nickel ribbon with a weak acid solution of $Mg(NO_3)_2$ (pH = 5.8), with the subsequent drying and calcination, may be accompanied by corrosion of nickel with the transition of Ni^{2+} cations into solution. These cations can be incorporated into the bulk of MgO particles.

TEM data indicate that in reduced catalysts, crystallites of supported nickel are dispersal (3-7 nm) (Table 2) and epitaxially bound with MgO[36,39] (Fig. 4): the image of nickel particles exhibits a moire fringe pattern in the form of parallel fringes with a period of about 1 nm as a result of lattice spacing d_{111} of Ni and MgO superposition.[40] In catalysts, epitaxially unbound crystallites of supported nickel are very rare; these crystallites are oxidized and their surface contains a 1-2-nm layer of NiO. In catalysts, the epitaxially bound highly dispersed nickel crystallites less than 7 nm do not have the oxide layer after exposure to air.[21,36,39]

It is believed that in the studied catalysts, epitaxial binding of nickel crystallites with MgO is due to the formation of nickel crystallites from a solid solution of $Ni_XMg_{1-X}O$ and due to their high dispersion.

3.2. Catalytic activity

Figure 5 shows the activity of the prepared catalysts in the SCDR of methane. The conversion of methane over the initial nickel ribbon was 7% and decreased to 0.5% during the reaction, apparently because of carbonization. The supporting of the MgO underlayer on the initial nickel ribbon increases the conversion of methane to 56% (support I). The increase in conversion can be attributed to the interaction of NiO and MgO with the formation of the dispersed mixed oxide, from which dispersed nickel crystallites are formed under the influence of the reaction medium.[21]The increase in activity is also facilitated by loosening of the nickel ribbon surface during the heating in the presence of nitrogen oxides, which are formed by the decomposition of $Mg(NO_3)_2$, and subsequent reduction in hydrogen.[26,27] During the reaction, the conversion on support I decreases; this can be caused by sintering of the loosened nickel ribbon and by its carbonization. As shown in Figure 3, in support I some parts of the nickel ribbon surface do not contact with the particles of MgO. It is known[41] that sintering of the particles by the surface diffusion mechanism starts at a temperature (the so-called Tamman temperature) which is much lower than the conventional melting point of a bulk material; this is caused by defectness of the near-surface layers of a solid. It is expected that under the influence of the reaction medium at 750°C, the parts of nickel ribbon in support I that are not covered with magnesium oxide undergo sintering by the surface diffusion mechanism.

Carbonization of nickel catalysts supported on α-Al_2O_3 and Al_2O_3-SiO_2 with a magnesium oxide underlayer was observed in SCDR of methane.[6,8,9] This suggests that the action of reaction medium on the regions of nickel ribbon in support I that are not covered with MgO leads to their carbonization.

The supporting of Ni (1.0 and 2.7 wt.%) onto the support I decreases its catalytic activity (Fig. 5); this can be explained as follow: upon impregnation of the support I with the aqueous solutions of nitrates

a substantial part of MgO is rehydrated;[39,40] earlier we have shown[21] that thermal treatment of nickel ribbon impregnated with a $Mg(NO_3)_2$ solution in N_2 flow at 550°C yields the MgO with a smaller specific surface area compared to its annealing in hydrogen; in the supported catalysts (1.0% Ni/(pNirb + 6.7% MgO) (I) and 2.7% Ni/(pNirb + 8.6% MgO) (I)) the supported nickel particles have the larger predominant size and the smaller surface area of metallic nickel than those in the support I.

In the supported catalysts with the increase in the content of supported nickel, the catalyst activity increases, which may result from an increase in the surface area of metallic nickel per unit weight of the catalyst (Fig. 5).

Figure 5 shows the effect of test duration on the conversion of methane. The decrease in the activity of catalyst I containing 1.0 % Ni/pNirb + 6.7 % MgO was about 20%. For comparison, Fig. 5 depicts the activity of the latter catalyst but reduced at 750ºC. The decrease in the activity of the catalysts reduced at 750 and 900ºC was comparable. The activity of catalysts I with high content of MgO (8.6 and 10.4 wt.%) and catalysts II remained stable throughout the test period.

The H_2/CO ratio in the reaction products over supported catalysts I with low content of MgO (6.7 вес.%) was 2.7-2.8, whereas for catalysts I with high content of MgO and catalysts II, this ratio was 2.1-2.2 and almost did not change during the reaction. An increased H_2/CO ratio (2.7-2.8) in the reaction products in the case of catalyst I with a low content of MgO (1.0% Ni/(pNirb + 6.7% MgO) (I)) may be caused by carbonization of some parts of the nickel ribbon surface which can be free from the MgO underlayer and a decrease in CO content in the reaction products.

For comparison, Figure 5 presents the effect of test duration on the conversion of methane over a commercial catalyst NIAP-18. These results show that supported catalysts I with high content of MgO and catalysts II on the highly thermally conductive support are comparable in activity with the catalyst NIAP-18 and surpass it in stability under conditions of SCDR of methane.

Table 3 lists the test data for the monolithic catalyst in SCDR of methane to synthesis gas performed in the developed flow reactor.

Table 3 Parameters of SCDR of methane to synthesis gas for the monolithic catalyst.

Flow rate, L/min			τ, s	T cat., °C			Product composition, %				CH_4 conversion, %
CH_4	H_2O	CO_2		T_7[1]	T_8[2]	T_9[3]	CH_4	CO_2	CO	H_2	

3.0	3.53	1.95	0.29	657	697	806	1.4	7.9	32	59	94	experimental	
							0.27	6.95	31.5	61.3	98.9	equilibrium[4]	
3.0	3.70	1.95	0.29	672	715	816	1.3	7.7	32	60	95	experimental	
4.50	2.90	5.20	0.20	696	742	809	3.7	11	29	57	86	experimental	
							0.28	6.80	31.7	61.2	98.8	equilibrium[4]	

[1] Thermocouple is mounted in the monolithic catalyst at a distance of 5 mm from the reaction mixture inlet. [2] Thermocouple is mounted in the monolithic catalyst at a distance of 15 mm from the reaction mixture inlet.[3] Thermocouple is mounted in the monolithic catalyst at a distance of 5 mm from the reaction mixture outlet.[4] The equilibrium values of methane conversion and synthesis gas yield correspond to the temperature of monolithic catalyst at the reactor outlet. Designations of thermocouples in Table 3 are in accord with Figure 1.

According to the test data, methane conversion on the monolithic catalyst at a contact time 0.29 s was not lower than 94 % and the synthesis gas yield was 90%; at this contact time experimental values are close to the calculated equilibrium values. The H_2/CO ratio in the reaction products over monolithic catalyst was close to 1,9. These results indicate that the monolithic catalyst based on 4.0% Ni/(pNirb + 10.4% MgO) (I) is an effective catalyst for the SCDR of methane to synthesis gas.

In studies[44-47] the structured catalysts based on metallic supports with oxide undelayer were used for the synthesis gas production by methane and liquefied fuels conversion. Noble metals,[44-47] nickel[45] and nickel doped with noble metals[44,45] were used as the active component. The active component containing mixed oxides of La, Ce, Zr and nickel doped with noble metals is considered as the most promising one for the development of monolithic catalysts for reforming of methane and liquefied fuels to synthesis gas.[44,48]

The test data in the reaction of partial oxidation of methane to synthesis gas for the monolithic catalyst based on 3.0% Ni/(rpNi + 5.0% MgO), whose composition is close to the catalysts studied in our paper, are presented in ref.[39]. The obtained values of methane conversion and synthesis gas yield are comparable with those reported for the same range of contact time and composition of the reaction mixture for the Pt-promoted Ni-containing active component supported on Fecralloy monolithic substrate.[49]

3.3. Texture of catalysts after tests in SCDR of methane

According to TEM data after the tests in catalysts I and II a small number of enlarged nickel crystallites (20-40 nm) appear, but the most of the supported nickel crystallites remain in the stable state of dispersed crystallites epitaxially bound with MgO. Some of these crystallites do not have the oxide film on their surface. Besides, there appear highly dispersed nickel crystallites (2-3 nm) epitaxially bound with MgO. In catalysts I with the high content of MgO, on large nickel particles (~ 100 nm) detached from the nickel support, there appear nickel crystallites of 5-10 nm in size epitaxially bound with MgO probably containing NiO (Fig. 6). In initial catalysts I with high content of MgO these crystallites were not found. These results indicate that in catalysts I with high content of MgO under the influence of the reaction medium, there proceeds a reduction of nickel oxide from the hardly reducible solid solution NiO-MgO, which is formed on the surface of the nickel ribbon.

In the supported catalysts I and II the formation of dispersed solid solution and mixed oxide is facilitated both by the supporting of nickel from a mixture of $Ni(NO_3)_2$ and $Mg(NO_2)_2$ solutions and by treatment in hydrogen at 900°C, which increases the diffusion mobility of cations and intensifies the incorporation of Ni^{2+} cations into the lattice of MgO and Mg^{2+} cations into the lattice of NiO; the reduction of NiO from the solid solution and mixed oxide leads to the formation of dispersed nickel crystallites; unreduced part of the solid solution and mixed oxide may disperse the nickel particles.

The treatment under reaction conditions of catalyst I with low content of MgO (1.0 wt.% Ni/pNirb+6.7% MgO) does not result in the formation of carbon on dispersed nickel crystallites epitaxially bound with MgO. However, the islet formation of graphite-like carbon was observed on the large particles of nickel (~ 100 nm) detached from the nickel support. It is known[22,31,50] that large nickel particles are more prone to carbonization than small ones. As shown in Figure 3, in support I some parts of the nickel ribbon surface do not contact the particles of MgO. Because the content of MgO in catalyst I (1.0 wt.% Ni/pNirb+6.7% MgO) was increased insignificantly compared with the support I, one can suppose that some parts of the nickel support surface can be free from the MgO underlayer. When exposed to the reaction medium, these parts can be carbonized. Thus, the observed decrease in the activity of catalyst I with low content of MgO can be attributed to the carbonization of large crystallites of the nickel ribbon that are not covered with MgO.

Catalysts I with high content of MgO and catalysts II exhibited stable activity and contained no carbon deposits after reaction. Their resistance to carbonization is possibly a result of the formation of dispersed nickel crystallites epitaxially bound with MgO, as well as result of the formation of the MgO underlayer, which covers completely the nickel ribbon and prevents the contact of the reaction medium with large nickel crystallites and thus prevents their carbonization. It is known[1,3,6-10] that during the SCDR of methane, nickel catalysts are inclined to carbonization. TEM investigation of our catalysts showed that no carbon is deposited on nickel crystallites epitaxially bound with MgO. In studied catalysts, a

considerable part of supported nickel crystallites is formed during the reduction of the solid solution of NiO in MgO (Table 1). It can be supposed that there is the interaction of these crystallites with MgO. The interaction of dispersed nickel crystallites with MgO can be indicated by their epitaxial binding and by the absence of the oxide layer on their surface. In this case, the catalytic properties of the catalyst are no longer determined only by supported metal, but refer to a unified system "metal-support" and depend on the nature of the support and the nature of its interaction with the metal.[51,52] It is believed that the epitaxial binding of nickel with MgO leads to a change in the catalyst properties and suppresses its activity in the reactions leading to the formation of carbon.[53]

An increased resistance to carbonization of the catalysts in the case when the precursor of the active component is a solid solution of NiO in MgO is shown in.[5,31,35,54] It is supposed that the carbon deposition is suppressed due to the formation of highly dispersed crystallites of nickel that are in interaction with MgO.[5,28] According to,[55] the formation of the partially reducible solid solution of NiO in MgO increases the stability of Ni–Ni bonds on the reduced surfaces; this higher surface stability inhibits carbon diffusion into the nickel lattice, and thus prevents the formation of carbon. Resistance to carbonization may also increase because of the basic properties of the surface of MgO: owing to the presence of labile hydroxyl groups[56-58] and activated molecules of CO_2,[59] which oxidize hydrocarbon fragments.

4. Conclusion

In the nickel catalysts supported on a porous nickel ribbon with the MgO underlayer, nickel crystallites are epitaxially bound with MgO and some of the dispersed nickel crystallites do not have an oxide film on their surface. It is believed that the epitaxial binding of nickel with MgO leads to a change the catalyst properties and suppresses its activity in the reactions leading to the formation of carbon. When tested in the SCDR of methane, the catalysts with the MgO underlayer completely covering the nickel ribbon exhibit a stable activity; no carbon deposits are found in them.

The formation of dispersed nickel crystallites epitaxially bound with MgO and the formation of the MgO underlayer, which covers the nickel ribbon, prevents its contact with the reaction medium and thus prevents its carbonization, can determine the stability of these catalysts.

Acknowledgements

The authors thank V.A.Kirillov, N.A.Kuzin, Yu.I.Amosov, A.B.Shigarov, N.F.Saputina for help in this work. This work was supported by the Russian Foundation of Basic Research (grant 15-03-04001).

References

1. V. R. Choudhary, A. M. Rajput, *End.Eng.Chem.Res.,* 1996, **35**, 3934.
2. V. R. Choudhary, K. C. Mondal, *Appl.Energy,*2006, **83**, 1024.
3. H.-S. Roh, K. Y. Koo, J. H. Jeong, Y. T. Seo, D. J. Seo, Y. S. Seo, W. L. Yoon, S. B. Park, *Catal.Lett*., 2007, **117**, 85.
4. F. Pompeo, N. N. Nichio, M. M. V. M.Souza, D. V.Cesar, O. A. Ferretti, M. Schmal, *Appl. Catal. A: Gen,* 2007, **316**, 175.
5. M. C. J. Bradford, M. A. Vannice, *Catal. Rev. Sci. Eng*., 1999, **416**,1.
6. J. Mehz, K. J. Jozani, A. N. Pour, Y. Zamani, *React. Kinet. Catal. Lett*., 2002, **75**, 267.
7. O. Yamazaki, T. Nozaki, K. Omata, K. Fujimoto, *Chem.Lett*., 1992, **21**, 1953.
8. V. R. Choudhary, B. S. Uphade, A. S. Mamman, *Catal. Lett*., 1995, **32,** 387.
9. V. R. Choudhary, B. S. Uphade, A. S. Mamman, *Appl. Catal. A: Gen*., 1998, **168**, 33.
10. K. Tomishige, Y. Himeno, O. Yamazaki, Y. Chen, K. Fujimoto, *Kinet.Catal*., 1999, **40**, 432 (in Russian).
11. K. Y. Koo, H-S Roh, U. H. Jung, D. J. Seo, Y-S Seo, W. L. Yoon, *Catal.Today,* 2009, **146**, 166.
12. M. Garcia-Dieguez, I. S. Pieta, M. C. Herrera, M. A. Larrubia, L. J. Alemany, *Catal.Today,* 2011, **172,** 136.
13. K. Takanabe, K. Nagaoka, K. Nariair, K. Aika, *J.Catal*., 2005, **230**, 75.
14. I. H. Son, S. J. Lee, A. Soon, H.-S. Roh, H. Lee, *Appl. Catal. B: Env*., 2013, **134-135**, 103.
15. M. Sheng, H. Yang, D. Cahela, B. J. Tatarchuk, *J.Catal*., 2011, **281**, 254.
16. T. Boger, A. K. Herbel, *Chem.Eng. Sci*., 2005, **60,** 1823.
17. V. A. Kirillov, N. A. Kuzin, A. V. Kulikov, S. I. Fadeev, A. B. Shigarov, V. A. Sobyanin, *Teor. Osn. Khim. Tekhnol.,* 2003, **37**, 300.
18. M. M. Danilova, Z. A. Sabirova, N. A. Kuzin, V. A. Kirillov, N. A. Rudina, E. M. Moroz, A. I. Boronin, *Kinet.Catal.*, 2007, **48**, 121 (in Russian).
19. Z. R. Ismagilov, B. B. Pushkarev, N. A. Koryabkina, H. Veringa, *Chem. Eng. J,.* 2001, **82**, 355.
20. Yu. V. Potapova, *Cand. Sci. (Chem.) Dissertation*, Novosibirsk: Boreskov Inst. of Catalysis, 2002.
21. Z. A. Sabirova, M. M. Danilova, V. I. Zaikovskii, N. A. Kuzin, V. A. Kirillov, T .A. Krieger, V. D. Meshcheryakov, N. A. Rudina, O. F. Brizitskii, L. N. Khrobostov, *Kinet.Catal.,* 2008, **49**, 449 (in Russian).
22. Y. H. Hu, E. Ruckenstein, *Catal. Rev.Sci.Eng*., 2002, **44**, 423.
23. A. Shamsi, J. J. Spivey, *Ind.Eng.Chem.Res*., 2005, **44**, 7298.
24. G. F. Tikhonov, L. A. Pyryalov, V. K. Sorokin, *Powder Metall*., 1973, **12,** 85 (in Russian).
25. G. Chen, K. Tomishige, K. Fujimoto, *Appl. Catal A.: Gen*., 1997, **161,** 11.
26. I. M. Bodrov, L. O. Apel'baum, M. I. Temkin, *Kinet.Catal*., 1964, **5**, 696 (in Russian).
27. L. J. I. Coleman, E. Croiset, W. Epling, M. Fowler, R. R. Hudgins, *Catal. Lett*., 2009, **128**, 144.

28. V. I. Yagodkin, Yu. T. Fedyukin, V. N. Men'shov, and V. A. Daut, *Khim. Prom–st.,* 2001, **2**, 7.
29. JCPDS Data File No. 45–0946.
30. JCPDS Data File No. 47–1049.
31. Y. H. Hu, E. Ruckenstein, *Catal.Lett.,* 1997, **43**, 71.
32. T.Yoshida, T.Tanaka, H.Yoshida, T.Funabiki, S.Yoshida, *J.Phys.Chem*., 1996, **100**, 2302.
33. M.Serra, P.Salarge, Y.Cestores, F.Medina, J.E.Sueiras, *Solid State Ionics*, 2000, **134**, 229.
34. *Handbook of Chemistry, Khimiya, Leningrad*, 1971, **1**, 786 (in Russian).
35. O. Yamazaki, K. Tomishige, K. Fujimoto, *Appl. Catal. A: Gen*., 1996, **136,** 49.
36. M. M. Danilova, Z. A. Fedorova, V. I. Zaikovskii, A. V.Porsin, V. A. Kirillov, T. A. Krieger. *Appl.Catal.B: Env*., 2014, **147**, 858.
37. G. C. Bond, S. P. Sarsam., *Appl. Catal. A.: Gen*., 1988, **38**, 365.
38. N. Takezawa, H. Terunuta, M. Shimokawabe, H. Kobayashi, *Appl. Catal. A.: Gen.,* 1986*,* **23**, 291.
39. V. A. Kirillov, Z. A. Fedorova, M. M. Danilova et al., *Appl. Catal A.: Gen*., 2011, **401**, 170.
40. P. B. Hirsch, A. Howie, R. B. Nickolson et al. *Electron Microscopy of Thin Crystals*, Butterworths, 1965.
41. Ya.E. Geguzin, *Physics of sintering,*, Moscow, 1967, 310.
42. M. A. Aramendia, V. Boran, C. Jimenez, *Appl. Catal. A.: Gen*., 2003, **244**, 207.
43. E. Hillerova, Vit. Zdrazil, *Appl. Catal A: Gen*., 1994, **118**, 111.
44. V. Sadykov, V. Sobyanin, N. Mezentseva, G. Alikina et al., *Fuel*, 2010, **89**, 1230.
45. Y. Guo, L. Zhou, H. Kameyama, *Int.J.Hydr.Energy*, 2011, **36,** 5321.
46. H-S Roh, D. K. Lee, K. Y. Koo, U. H. Jung, W. L. Yoon, *Int.J.Hydr.Energy,* 2010, **35**, 1613.
47. W. Cai, F. Wang, A.van Veen, C. Descorme, Y. Schuurman, W. Shen, C. Mirodatos, *Int.J.Hydr.Energy*, 2010, **35**, 1152.
48. V. A. Sadykov, S. N. Pavlova, R. V. Bunina, G. M. Alikina, S. F. Tikhov, at al., *Kinet.Katal*., 2005, **46**, 243.
49. V. Sadykov, S. Pavlova, O. Snegurenko et al., *Stud. Surf. Sci. Catal*., 2007, **172**, 241.
50. K. Tomishige, G.Chen, K. Fujimoto, *J.Catal.,* 1999, **181**, 91.
51. L. M. Plyasova, T. M. Yurieva, T. A. Krieger, O. V. Makarova, V. I. Zaikovskii, L. P. Solovyeva, A. N. Shmakov, *Kinet. Catal*., 1995, **36**, 464.
52. G. K. Boreskov, *Theoretical Problems of Catalysis*, USSR Academy of Sciences, Siberian Branch, Institute of Catalysis, Novosibirsk, 1977, 113.
53. A. R. Kaul, O. Yu. Gorbenko, A. A. Kamenev, *Russ.Chem.Rev*., 2004, **73**, 932.
54. Y. Chen, K. Tomishige, K. Yokogama, K. Fujimoto, J.Catal., 1999, **184**, 479.
55. M. C. J. Bradford, M. A. Vannice, *Appl. Catal. A: Gen.,* 1996, **142,** 73.
56. J. Wei, E. Iglesia, *J.Catal*., 2004, **224**,370.
57. K. Polychronopoulou, C.N. Costa, A.M. Estaphiou, *Catal. Today,* 2006, **112**, 89.
58. J. M. Aparicio, *J.Catal*., 1997, **165**, 262.

59. G. S. Gallego, C. Baliot-Dupeyrat, J. Barrault, E. Florer, F. Mondragon, *Appl. Catal.A: Gen*., 2008, **334**, 251.

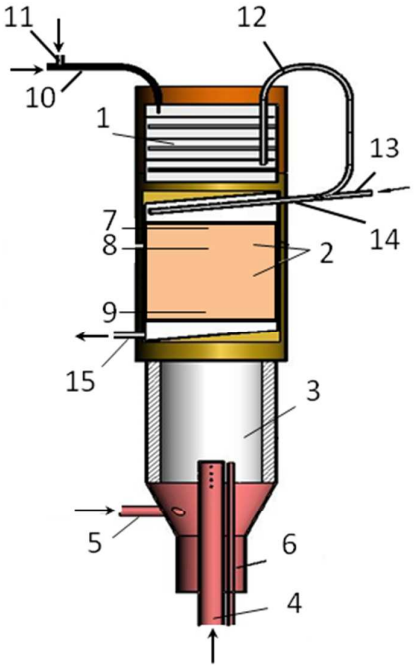

Fig.1 Scheme of reactor for the monolithic nickel catalyst testing in SCDR of methane to synthesis gas: 1 – evaporator, 2 – monolithic catalyst, 3 – gas burner, 4 – fuel mixture inlet, 5 – additional flow air inlet, 6 – electrode, 7,8,9 – thermocouples mounted in monolithic catalyst, 10 – water inlet, 11 – carbon dioxide inlet, 12 – steam and carbon dioxide mixture inlet, 13 – methane inlet, 14 – reaction mixture inlet, 15 – reaction product outlet.

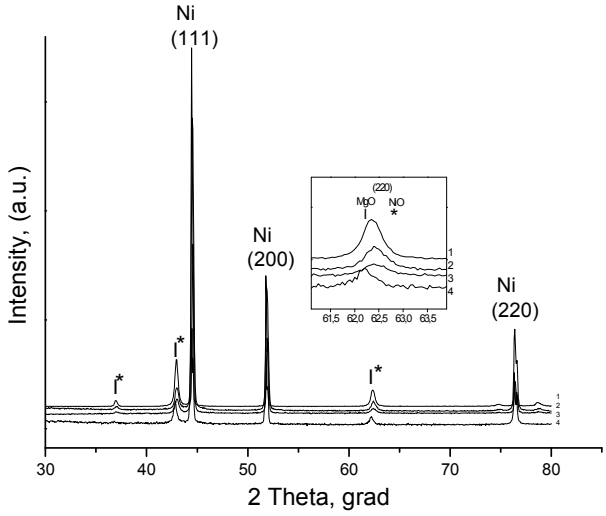

Fig.2. XRD pattern of samples: 1 - 2.3% Ni/(pNirb + 12.2% MgO) (II), 900ºC, H_2; 2 – 4.0% Ni/(pNirb + 10.4% MgO) (I), 900ºC, H_2; 3 – 2.7%Ni/ (pNirb + 8.6% MgO) (I), 900ºC, H_2; 4 – pNirb + 6.0% MgO (I), 550ºC, H_2. The insert – fragment of XRD patterns of samples. Denoted as (|) and (*) location of diffraction peaks of MgO and NiO, respectively.

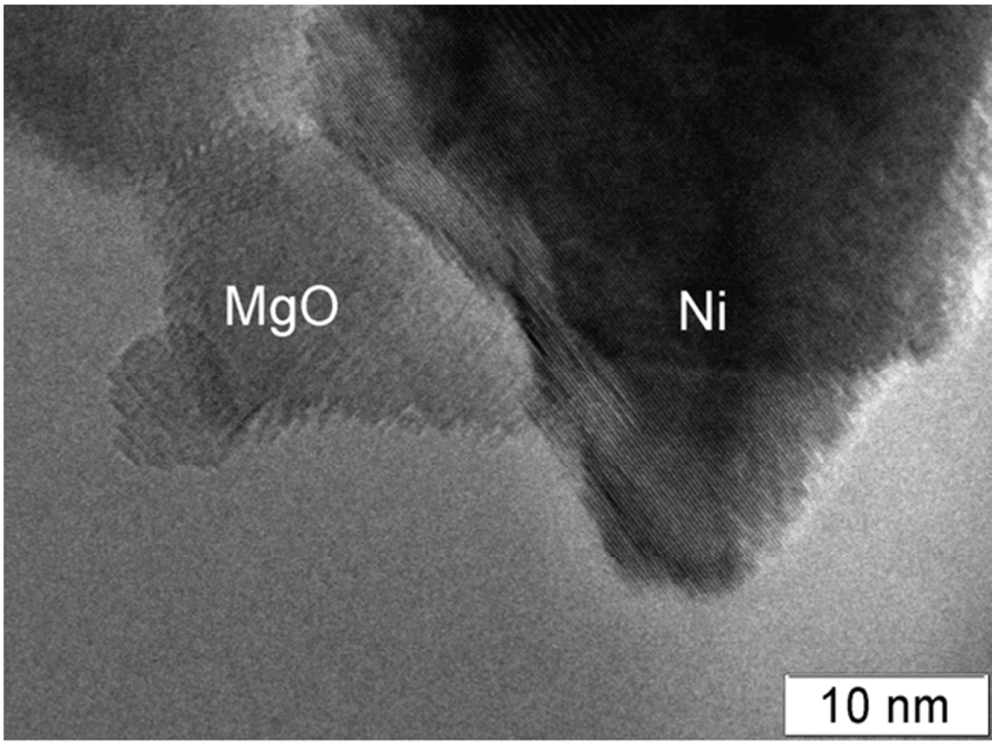

Fig. 3. HRTEM image of the nickel ribbon with MgO underlayer (support I), 550°C, H_2.[36]

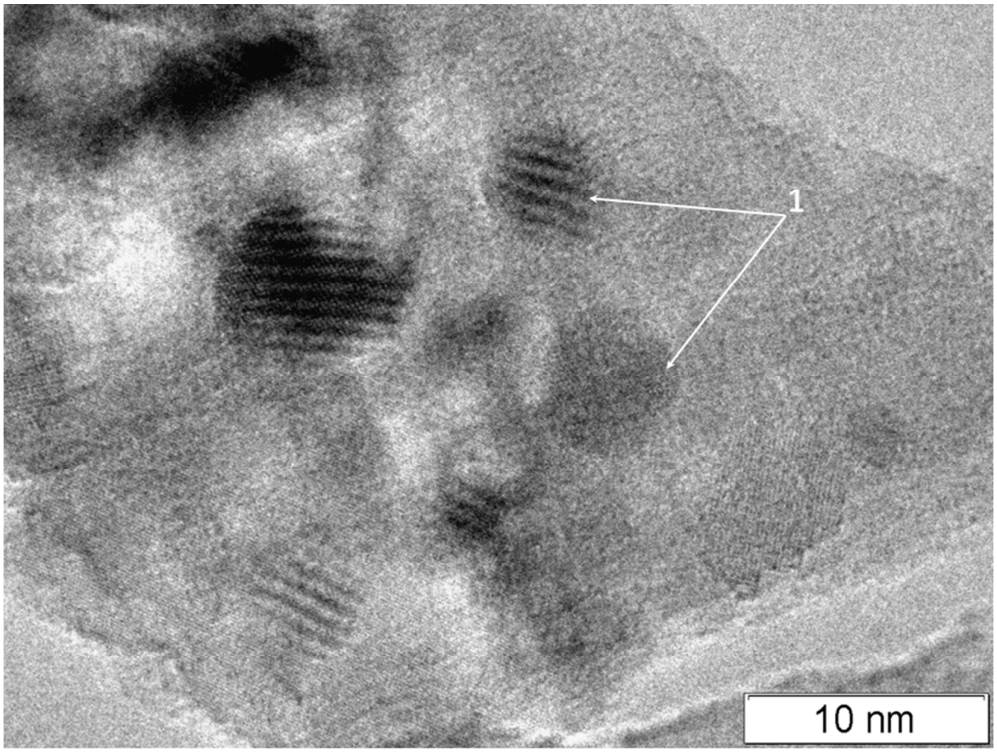

Fig.4. HRTEM image of the catalyst 2.7 % Ni/(pNirb+8.6% MgO) (I), 900°C, H_2 (1 - dispersed nickel crystallites epitaxially bound with MgO).

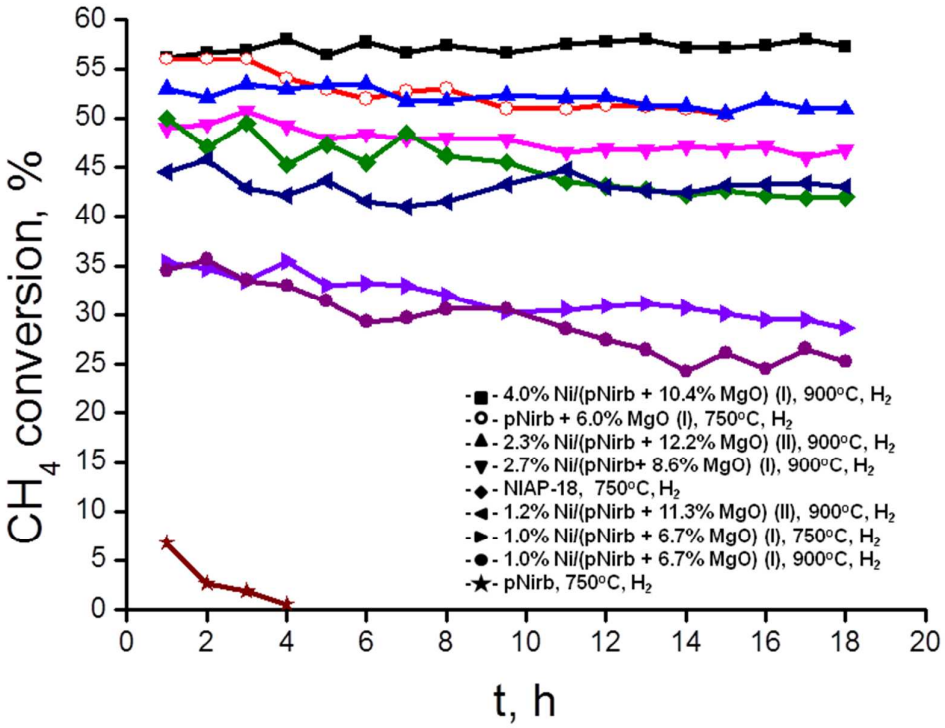

Fig.5. Methane conversion versus time-on-stream in the steam-CO_2 reforming of methane to synthesis gas over the catalysts reduced in H_2 (T = 750°C, p = 1 atm, $CH_4/CO_2/H_2O/N_2$ = 35/23/39/3, weight of catalyst: 0,40 g).

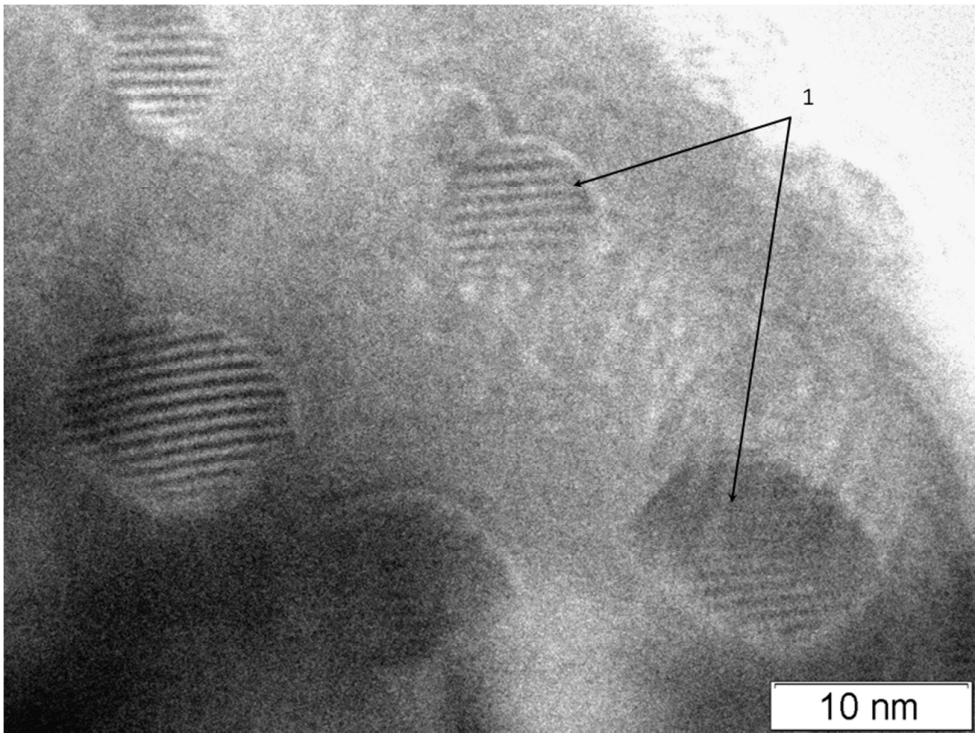

Fig.6. HRTEM image of the catalyst 4.0% Ni/(pNirb + 10.4% MgO) (I) tested in the steam-CO_2 reforming of methane (1 - dispersed nickel crystallites epitaxially bound with MgO).